UCLA
UCLA Previously Published Works

Title

Axonal damage in spinal cord is associated with gray matter atrophy in sensorimotor cortex in experimental autoimmune encephalomyelitis

Permalink

https://escholarship.org/uc/item/7ww7s5bx

Journal

Multiple Sclerosis Journal, 26(3)

ISSN

1352-4585

Authors

Meyer, Cassandra E
Gao, Josephine L
Cheng, James Ying-Jie
et al.

Publication Date

2020-03-01

DOI

10.1177/1352458519830614

Peer reviewed

eScholarship.org Powered by the California Digital Library
University of California

Author Manuscript

Author Manuscript

Author Manuscript

Author Manuscript

HHS Public Access

Author manuscript

Mult Scler. Author manuscript; available in PMC 2021 March 01.

Published in final edited form as:

Mult Scler. 2020 March ; 26(3): 294–303. doi:10.1177/1352458519830614.

Axonal damage in spinal cord is associated with gray matter atrophy in sensorimotor cortex experimental autoimmune encephalomyelitis

Cassandra E. Meyer[a,b], **Josephine L. Gao**[a,b], **James Ying-Jie Cheng**[a,b], **Mandavi R. Oberoi**[a,b], **Hadley Johnsonbaugh**[a,b], **Stefano Lepore**[a,b], **Florian Kurth**[a,b], **Mackenzie J. Thurston**[a,b], **Noriko Itoh**[b], **Kevin R. Patel**[b], **Rhonda Voskuhl**[a,b], **Allan MacKenzie-Graham**[a,b,*]

[a]Ahmanson-Lovelace Brain Mapping Center, Department of Neurology, David Geffen School of Medicine at UCLA, Los Angeles, CA, USA

[b]UCLA Multiple Sclerosis Program, Department of Neurology, David Geffen School of Medicine at UCLA, Los Angeles, CA, USA

Abstract

Background—Gray matter (GM) atrophy in brain is one of the best predictors of long-term disability in multiple sclerosis (MS) and recent findings have revealed that localized GM atrophy is associated with clinical disabilities. GM atrophy associated with each disability mapped to a distinct brain region; revealing a disability-specific atlas (DSA) of GM loss.

Objective—To uncover the mechanisms underlying the development of localized GM atrophy.

Methods—We used voxel-based morphometry (VBM) to evaluate localized GM atrophy and Clear Lipid-exchanged Acrylamide-hybridized Rigid Imaging-compatible Tissue-hYdrogel (CLARITY) to evaluate specific pathologies in mice with experimental autoimmune encephalomyelitis (EAE).

Results—We observed extensive GM atrophy throughout the cerebral cortex, with additional foci in the thalamus and caudoputamen, in mice with EAE compared to normal controls. Next, we generated pathology-specific atlases, voxelwise mappings of the correlation between specific pathologies and localized GM atrophy. Interestingly, axonal damage (end-bulbs and ovoids) in the spinal cord strongly correlated with GM atrophy in the sensorimotor cortex of the brain.

Conclusions—The combination of VBM with CLARITY in EAE can localize GM atrophy in brain that is associated with a specific pathology in spinal cord; revealing a pathology-specific atlas (PSA) of GM loss.

Keywords

Voxel-based morphometry; CLARITY; EAE; MS; neurodegeneration; axonal loss

[*]Corresponding Author: Allan MacKenzie-Graham, PhD, Department of Neurology, David Geffen School of Medicine at UCLA, 635 Charles Young Drive South, Suite 225-Z, Los Angeles, CA 90095-7334, Phone: (310) 267-5153, amg@ucla.edu.

Disclosures

The content is solely the responsibility of the authors and does not necessarily represent the official views of the National Institutes of Health. The authors report no conflicts of interest relating to this publication.

Author Manuscript Author Manuscript Author Manuscript Author Manuscript

Introduction

Multiple sclerosis is an autoimmune-mediated disease of the central nervous system characterized by demyelination, axonal damage, and synaptic loss.[1] While MS has long been regarded as a disease of white matter (WM), gray matter (GM) atrophy has a direct relationship with clinical outcomes.[2–4]

Voxel-based morphometry (VBM) is an effective method of analyzing localized GM atrophy in a biology-driven manner, as opposed to focusing on a priori selected structures. In VBM, statistical analyses are conducted throughout the entire brain on a voxelwise basis,[5] permitting localization of volume changes across neuroanatomical structures. Voxelwise analyses have been conducted extensively in MS and have provided valuable insights into the pattern and progression of GM atrophy.[4, 6–8] VBM is particularly well-suited in MS because GM atrophy is not homogenously distributed throughout the brain. For example, atrophy within sensorimotor cortex was shown to correlate with worse scores on the Expanded Disability Status Scale (EDSS), a composite heavily weighted by walking disability.[8] Furthermore, our group has used VBM to generate disability-specific atlases (DSAs), voxelwise mappings of GM atrophy in the cerebral cortex that are associated with specific disabilities. We showed that GM atrophy in distinct, clinically-eloquent cortical regions correlated with distinct disabilities, such as atrophy in the primary auditory cortex with poorer performance on the paced auditory serial addition test (PASAT).[2] These studies illustrate the need to further understand the mechanisms contributing to regional GM atrophy. Investigating these mechanisms is challenging in humans, but they can readily be addressed through the use of animal models, such as experimental autoimmune encephalomyelitis (EAE).

Clear Lipid-exchanged Acrylamide-hybridized Rigid Imaging-compatible Tissue-hYdrogel (CLARITY) is an optical clearing technology that permits intact imaging of the entire brain and spinal cord.[9] This approach is well-suited to visualizing neurons and axons in three dimensions, in both brain and spinal cord, in both normal and pathological conditions,[9, 10] such as in EAE.[11] Thus, CLARITY can be utilized to visualize pathological mechanisms across the neuraxis that may lead to GM atrophy. In fact, different cellular pathologies may be responsible for atrophy in different brain regions. This may explain the difficulty in uncovering the underlying mechanism of whole GM atrophy – there is not one mechanism, but many.

Here, we will focus on an important candidate mechanism, axonal damage in the spinal cord. In order to visualize the relationship between GM atrophy and axonal damage, a voxelwise regression analysis was conducted and a mapping of GM atrophy in the cerebral cortex that was associated with axonal damage in the spinal cord was created – a pathology-specific atlas (PSA).

Author Manuscript Author Manuscript Author Manuscript Author Manuscript

Materials and Methods

Mice

18 female Thy1-YFP$^+$ C57BL/6J mice with EAE and 17 female age-matched, healthy controls (Jackson Laboratories, Bar Harbor ME) ranging from 11 to 15 weeks of age were used for this study. All procedures were performed in accordance to the guidelines of the National Institutes of Health and the Chancellor's Animal Research Committee of the University of California, Los Angeles Office for the Protection of Research Subjects.

Experimental Autoimmune Encephalomyelitis

EAE was induced as described.[11] Briefly, mice were immunized subcutaneously with MOG peptide 35–55 (300 μg) and Mycobacterium tuberculosis (500 μg) emulsified in complete Freund's adjuvant, in a volume of 0.1 ml over the right draining inguinal and axillary lymph nodes. One week later, a booster immunization was delivered subcutaneously over the contralateral lymph nodes. Pertussis toxin (500 ng; List Biological Laboratories, Campbell, CA) was injected intraperitoneally on days 0 and 2.[12] EAE was graded on a scale of 0–5, as described.[13]

Magnetic Resonance Imaging

All animals were scanned *in vivo* 20 days after EAE induction at the Ahmanson-Lovelace Brain Mapping Center at UCLA on a 7T imaging spectrometer (Bruker Instruments, Billerica, MA), as described.[14]

Voxel-based Morphometry

VBM analyses were performed with Statistical Parametric Mapping (SPM) 8 software (Welcome Trust Center for Neuroimaging, London, United Kingdom; http://www.fil.ion.ucl.ac.uk/spm) and SPMMouse (SPMMouse, http://www.spmmouse.org) [15] within MATLAB version 2013a (Mathworks, Natick, MA). MR images were manually registered to tissue probability maps (TPMs) generated from 60 C57BL/6J mice [14] using 6-parameter linear transformations. The images were bias corrected and segmented into GM, WM, and cerebrospinal fluid (CSF) using the unified segmentation algorithm.[16] The resulting segments were used to create a Diffeomorphic Anatomical Registration using Exponentiated Lie algebra (DARTEL) template [17] and the individual GM segments were warped to this template and modulated. Finally, the normalized and modulated GM segments were smoothed with a 600 μm FWHM Gaussian kernel and used as the input for the statistical analysis.

Cross-sectional differences in local GM volume between EAE and control mice were examined with a general linear model. Whole brain volume was included as a covariate to account for the variance associated with brain size and to prevent potential effects due to differences in brain size. Within this model, significant differences in local GM volume between groups were determined via student's t-tests. All findings were corrected for multiple comparisons by controlling the false discovery rate (FDR) [18] and all significance maps were thresholded at $q \leq 0.05$. All analyses were performed bi-directionally.

Author Manuscript Author Manuscript Author Manuscript Author Manuscript

Associations of voxelwise GM volumes with axonal end-bulbs and ovoids using voxelwise regression analyses were assessed within the general linear model. Whole brain size was included as a variable of no interest. All significant findings were corrected for multiple comparisons by controlling the FDR.

Bias-corrected images were skull-stripped, warped to the DARTEL template, and averaged to create a mean template for visualization.

Atlas-based Morphometry

A minimum deformation atlas (MDA) was created using the MR images from all subjects and anatomical structures were manually labelled on the MDA using BrainSuite 16a [19] (http://brainsuite.org) as described.[20] The labels were then warped out to the individual images and manually corrected by an investigator blind to each treatment group.

CLARITY

The brains from a subset (9 EAE mice and 10 normal controls) and spinal cords from all of the animals were optically cleared using the CLARITY protocol modified for "passive clearing" as described.[11]

Immunohistochemistry

The brains of a subset of animals (5 EAE mice and 5 normal controls) were stained using immunohistochemistry (IHC) as described.[20] Tissues were stained for either NeuroTrace (Invitrogen), myelin basic protein (MBP) (Aves), major histocompatibility complex II (MHC-II) (BioLegend), and/or ionized calcium-binding adapter molecule 1 (Iba1) (Wako).

Microscopy

Laser scanning confocal microscopy was performed at the California NanoSystems Institute (CNSI) Advanced Light Microscopy/Spectroscopy Shared Resource Facility at UCLA as described.[11, 20]

CLARITY Analysis

Automated cell counting in Imaris (Bitplane, Belfast, United Kingdom) was used to analyze the number of cortical layer V pyramidal neurons in the sensorimotor cortex. Spinal cord images were visualized and processed using FIJI (https://fiji.sc) as described.[11]

Statistical Analyses

ABM, CLARITY, and immunohistochemistry data were analyzed in R (https://www.r-project.org). Two-group comparisons were conducted using a student's t-test (two-tailed). Regression analyses are reported as Spearman correlation coefficients. All reported p values are corrected for multiple comparisons by controlling for the FDR. 95% confidence intervals for mean values are reported in brackets and were found by resampling (10,000 bootstraps).

Author Manuscript Author Manuscript Author Manuscript Author Manuscript

Results

Gray matter atrophy

In vivo MRI scans were collected from 18 female mice with EAE and 17 female, age-matched normal controls 20 days after disease induction (Fig. 1). VBM was conducted to identify regions of significant GM volume change in mice with EAE ($p < 0.05$). A statistical parametric map (SPM) indicated substantial GM atrophy in the brains of mice with EAE compared to controls (Fig. 2A). Atrophy was observed primarily in the cerebral cortex with smaller clusters in the caudoputamen, cerebellum, and thalamus (Fig. 2B).

As a complementary approach, volumes were measured for whole brain, GM, WM, CSF, caudoputamen, cerebral cortex, cerebellum, and thalamus (Table 1). Mice with EAE demonstrated a decrease of 7.45% ($p = 0.0016$) in cerebral cortex volume, 3.15% ($p = 0.0052$) in caudoputamen volume, 2.32% ($p = 0.034$) in thalamus volume, and 2.27% ($p = 0.028$) in cerebellum volume compared to normal controls. Thus, this complementary approach corroborated our new findings of localized GM atrophy demonstrated by VBM (Fig. 2A & B). Further, EAE mice exhibited a 6.01% decrease in mean whole brain GM volume compared to controls ($p = 0.0020$). An analysis of whole brain WM and the corpus callosum volume revealed no significant difference between EAE mice and normal controls, consistent with our previous findings in the cerebellum. [21]

Axonal damage in the spinal cord

We then addressed whether an important candidate pathology, remote injury in spinal cord, was associated with localized GM atrophy in the cerebral cortex. We evaluated axonal transection (end-bulbs) and axonal injury (ovoids) in the spinal cord. Whole spinal cords were optically cleared, imaged, and analyzed (Fig. 2C & D). Mice with EAE exhibited a 5.3-fold increase in axonal end-bulbs compared to control mice ($p = 0.0063$) (Fig. 2E). Additionally, EAE mice also exhibited a 5-fold increase in axonal ovoids compared to controls ($p = 1.3 \times 10^{-9}$) (Fig. 2F).

We had previously created disability-specific atlases using MRI scans from MS patients in order to highlight the relationship between voxelwise GM atrophy and specific disabilities.[2] This biology-driven approach demonstrated that distinct disabilities were associated with GM atrophy in distinct, clinically-eloquent regions. Here, we created pathology-specific atlases using MRI scans in EAE mice to demonstrate the relationship between voxelwise GM atrophy and axonal damage in the spinal cord.

The spinal cord axonal-transection (end-bulbs) PSA showed a significant relationship with GM atrophy mainly within the primary and secondary motor cortex and much of the primary and supplemental somatosensory cortex (peak $p = 0.0036$, FDR corrected) (Fig. 2 G & H).[22] The total volume of this PSA was 11.2 mm^3. This result demonstrated that worse axonal transection in spinal cord correlates with worse GM atrophy in the sensorimotor cortex.

The spinal cord axonal-injury (ovoids) PSA exhibited a pattern very similar to the axonal-transection PSA, albeit smaller (6.64 mm^3), yet still significant (peak $p = 0.0093$, FDR corrected) (Fig. 2 I & J). The similarity between the axonal-transection PSA and the axonal-

Author Manuscript Author Manuscript Author Manuscript Author Manuscript

injury PSA was expected, given that there was a strong correlation between axonal end-bulbs and ovoids ($R = 0.754$, $p = 0.0016$).

Notably, each pathology-specific atlas (axonal transection, Figure 2 G & H, and axonal injury, Figure 2 I & J) was distinctly less widespread than overall voxelwise GM atrophy in mice with EAE (Figure 2 A & B), together demonstrating that GM atrophy associated with axonal damage in the spinal cord represents a subset of overall GM atrophy in the brain during EAE.

Neuronal loss in sensorimotor cortex

The neuroanatomic correlation between axonal transection in spinal cord and GM atrophy in sensorimotor cortex prompted investigation into cellular pathology in the sensorimotor cortex of mice with EAE. Thy1-YFP$^+$ mice express yellow fluorescent protein in a subset of their cortical layer V pyramidal neurons (Fig. 3A & B).[23, 24] Mice with EAE demonstrated a 44.7% reduction in cortical layer V pyramidal neurons in the sensorimotor cortex compared to controls ($p = 0.00028$) (Fig. 3C). As a complementary approach, we quantified NeuroTrace-labeled cells (all neurons) in the sensorimotor cortex in single tissue sections. We observed that mice with EAE showed a 13.7% reduction in cells labeled with NeuroTrace compared to controls ($p = 0.0063$) (Fig. 3C).

More loss of Thy1-YFP$^+$ neurons than NeuroTrace-labeled neurons in cerebral cortex is consistent with greater vulnerability of Thy1-YFP$^+$ neurons, since they are the source of Thy1-YFP$^+$ axons in spinal cord.[23] Indeed, there was a strong inverse correlation between the number of cortical layer V pyramidal neurons and the number of end-bulb positive axons ($R = -0.785$, $p = 0.028$), indicating a strong relationship between axonal transection in spinal cord and neuronal loss in sensorimotor cortex.

Demyelination and microglial activation in sensorimotor cortex

We evaluated demyelination within the sensorimotor cortex by immunohistochemistry (Fig. 4A & B). Mice with EAE exhibited a 32% reduction in MBP-staining compared to controls ($p = 0.00030$) (Fig. 4C).

There was a strong correlation between neuronal loss and myelin loss in the sensorimotor cortex ($R = 0.758$, $p = 0.028$), indicating that neuronal loss and myelin loss are closely related. Nevertheless, there wasn't a statistically significant correlation between end-bulb positive axons in the spinal cord and myelin loss in the sensorimotor cortex.

We assessed differences in activated microglia within the sensorimotor cortex in Iba1/MHC-II double-stained confocal images using morphology (Fig. 5A). We observed that mice with EAE exhibited a 3.5-fold increase in activated microglia compared to controls ($p = 0.017$) (Fig. 5B).

There was a strong direct correlation between the percentage of activated microglia and end-bulb positive axons ($R = 0.714$, $p = 0.042$), indicating a strong relationship between microglial activation in sensorimotor cortex and axonal transection in spinal cord. We also

Author Manuscript Author Manuscript Author Manuscript Author Manuscript

observed a strong indirect correlation between the percentage of activated microglia and neuronal numbers, both within sensorimotor cortex ($R = -0.733$, $p = 0.042$).

Discussion

It has been suggested that axonal damage is associated with whole GM atrophy in the brains of MS patients,[25] but localization of each has remained unclear. In this study, we used a biology-driven approach in the MS model, EAE, to reveal that axonal transection in spinal cord correlates strongly with GM atrophy in sensorimotor cortex. While we previously demonstrated that axonal transection in spinal cord correlated with atrophy of the whole cerebral cortex using atlas-based morphometry,[11] whether there were specific regions within the cerebral cortex that were associated with axonal transection in spinal cord was unknown. Here, we have developed a novel approach, pathology-specific atlases, mapping the relationship between localized GM atrophy and specific pathology, in effect localizing the impact of a specific pathology on GM in the brain.

These results extend previous studies from our lab demonstrating GM atrophy in discrete anatomical structures and neuronal loss in EAE.[11, 20, 21] In this study, we observed that axonal transection correlated strongly with Thy1-YFP$^+$ neuronal loss in the sensorimotor cortex. Together, our results suggest potential mechanisms underlying GM atrophy in EAE. Cortical layer V neurons in the sensorimotor cortex directly innervate the spinal cord through the corticospinal tract.[26, 27] The Thy1-YFP$^+$ axons that we analyzed in the spinal cord are projections from the Thy1-YFP$^+$ cortical layer V neurons in sensorimotor cortex.[23] We hypothesize that these long projections make them highly vulnerable to axonal injury and transection induced by inflammatory lesions along the length of the spinal cord, and that axonal injury and transection eventually lead to retrograde degeneration and cell death. Interestingly, in a mouse spinal cord injury model, axonal transection did not lead to Thy1-YFP$^+$ cortical layer V neuron loss in sensorimotor cortex,[28] suggesting that processes specific to EAE are responsible for neuronal loss. The remarkable specificity of the axonal-transection PSA suggests that distal axonal damage plays a key role in the development of GM atrophy in the sensorimotor cortex during EAE.

Notably, although the axonal-transection PSA was within the area of overall GM atrophy observed in EAE mice compared to normal controls (Figure 2 A & B), there were also large regions of GM atrophy that were not within this PSA (Figure 2 G & H). This suggests that while axonal transection in spinal cord correlates with atrophy within sensorimotor cortex, additional pathologies may also contribute to overall GM atrophy in EAE. Interestingly, GM atrophy in sensorimotor cortex after axonal transection in spinal cord injury models is controversial,[29] again suggesting that processes specific to autoimmune-mediated disease may be responsible for GM atrophy in EAE.

MS has GM atrophy in cerebral cortex and cortical lesions characterized by focal demyelination. However, the relationship between cortical lesions and atrophy of normal-appearing gray matter (NAGM) in cerebral cortex is unclear. We do not observe cortical lesions in EAE, but we do observe cortical GM atrophy, demonstrating that cortical GM atrophy need not be limited only to areas affected by cortical lesions.[30, 31]

Author Manuscript Author Manuscript Author Manuscript Author Manuscript

Consistent with the development of GM atrophy in NAGM of the cerebral cortex, our VBM analysis in EAE also identified localized atrophy in several deep GM structures including the anterior caudoputamen and the thalamus (Fig. 2). Voxelwise analyses have previously shown thalamus, caudate, and putamen atrophy in MS, particularly in the early stages. [6, 7, 32–34] Here, we are the first to show thalamic atrophy in EAE, suggesting that EAE may be a useful model to further investigate deep GM vulnerability to degeneration early in MS. Notably, although Tambalo et al. [35] detected atrophy in the caudoputamen in EAE in rats, they did not observe atrophy in thalamus. This difference may be due to the fact that Tambalo et al. used a relapsing-remitting EAE rat model, while we used a chronic EAE mouse model, although we cannot rule out technical differences.

The sensitive analyses used in this study allow us to detect atrophy and pathology earlier than has previously been observed, providing insight into the mechanisms responsible for early GM loss. It is likely that the processes contributing to GM atrophy will worsen as disease progresses and analyses at later timepoints would reveal greater atrophy in not only the cortical and deep GM structure highlighted in this study, but also in additional structures. For example, although we observed a 2.27% decrease in cerebellar volume, we anticipate greater cerebellar atrophy later in disease, as we have previously shown. [20, 21] Longitudinal studies will be useful for investigating the rate of progression of GM atrophy.

While our results are intriguing, our study has some limitations. Our voxelwise regression analyses are indicative of a strong relationship, but they are not necessarily causal. Future investigations of treatments to reverse individual pathologies and then determine the effect on their respective gray matter PSAs will reveal causality.

In summary, the combination of VBM with CLARITY has the potential to be an important tool in illuminating the underlying pathogenesis of GM atrophy in EAE and other neurodegenerative disease models. PSAs map the effects of specific pathologies on localized GM atrophy, acting as *in vivo* biomarkers for those pathologies by visualizing localized GM changes associated with each pathology. This approach can also be used to investigate neuroprotective treatments aimed at reducing axonal damage and neuronal loss early in disease to prevent GM atrophy within neurological pathways.

Acknowledgments

Funding

This work was generously supported by NINDS/NIH R01NS086981 (AMG), the Conrad N. Hilton Foundation [20150232 (RRV and AMG)], the Tom Sherak MS Hope Foundation (RRV), the Rhoda Goetz Foundation for MS (RRV), and by the Achievement Rewards for College Students (ARCS) Foundation (CEM). The authors are grateful for the generous support from the Brain Mapping Medical Research Organization, Brain Mapping Support Foundation, Pierson-Lovelace Foundation, The Ahmanson Foundation, Capital Group Companies Charitable Foundation, William M. and Linda R. Dietel Philanthropic Fund, and Northstar Fund. Research reported in this publication was also partially supported by the National Center for Research Resources and by the Office of the Director of the National Institutes of Health under award numbers C06RR012169, C06RR015431 and S10OD011939.

Author Manuscript Author Manuscript Author Manuscript Author Manuscript

References

1. Dendrou CA, Fugger L and Friese MA. Immunopathology of multiple sclerosis. Nat Rev Immunol 2015; 15: 545–558. 2015/08/08. DOI: 10.1038/nri3871. [PubMed: 26250739]
2. MacKenzie-Graham A, Kurth F, Itoh Y, et al. Disability-Specific Atlases of Gray Matter Loss in Relapsing-Remitting Multiple Sclerosis. JAMA Neurol 2016; 73: 944–953. 2016/06/14. DOI: 10.1001/jamaneurol.2016.0966 2527560 [pii]. [PubMed: 27294295]
3. Fisniku LK, Chard DT, Jackson JS, et al. Gray matter atrophy is related to long-term disability in multiple sclerosis. Ann Neurol 2008; 64: 247–254. 2008/06/24. DOI: 10.1002/ana.21423. [PubMed: 18570297]
4. Kuceyeski AF, Vargas W, Dayan M, et al. Modeling the relationship among gray matter atrophy, abnormalities in connecting white matter, and cognitive performance in early multiple sclerosis. AJNR Am J Neuroradiol 2015; 36: 702–709. 2014/11/22. DOI: 10.3174/ajnr.A4165. [PubMed: 25414004]
5. Ashburner J and Friston KJ. Voxel-based morphometry--the methods. Neuroimage 2000; 11: 805–821. 2000/06/22. DOI: 10.1006/nimg.2000.0582 S1053-8119(00)90582-2 [pii]. [PubMed: 10860804]
6. Datta S, Staewen TD, Cofield SS, et al. Regional gray matter atrophy in relapsing remitting multiple sclerosis: baseline analysis of multi-center data. Multiple sclerosis and related disorders 2015; 4: 124–136. 2015/03/20. DOI: 10.1016/j.msard.2015.01.004. [PubMed: 25787188]
7. Ceccarelli A, Rocca MA, Pagani E, et al. A voxel-based morphometry study of grey matter loss in MS patients with different clinical phenotypes. Neuroimage 2008; 42: 315–322. 2008/05/27. DOI: S1053–8119(08)00502–8 [pii] 10.1016/j.neuroimage.2008.04.173. [PubMed: 18501636]
8. Prinster A, Quarantelli M, Lanzillo R, et al. A voxel-based morphometry study of disease severity correlates in relapsing-- remitting multiple sclerosis. Mult Scler 2010; 16: 45–54. 2009/12/24. DOI: 10.1177/1352458509351896. [PubMed: 20028706]
9. Chung K, Wallace J, Kim SY, et al. Structural and molecular interrogation of intact biological systems. Nature 2013; 497: 332–337. 2013/04/12. DOI: 10.1038/nature12107 nature12107 [pii]. [PubMed: 23575631]
10. Lerner TN, Shilyansky C, Davidson TJ, et al. Intact-Brain Analyses Reveal Distinct Information Carried by SNc Dopamine Subcircuits. Cell 2015; 162: 635–647. 2015/08/02. DOI: 10.1016/j.cell.2015.07.014. [PubMed: 26232229]
11. Spence RD, Kurth F, Itoh N, et al. Bringing CLARITY to gray matter atrophy. Neuroimage 2014; 101: 625–632. 2014/07/20. DOI: 10.1016/j.neuroimage.2014.07.017 S1053-8119(14)00589-8 [pii]. [PubMed: 25038439]
12. Suen WE, Bergman CM, Hjelmstrom P, et al. A critical role for lymphotoxin in experimental allergic encephalomyelitis. J Exp Med 1997; 186: 1233–1240. [PubMed: 9334362]
13. Pettinelli CB and McFarlin DE. Adoptive transfer of experimental allergic encephalomyelitis in SJL/J mice after in vitro activation of lymph node cells by myelin basic protein: requirement for Lyt 1+ 2- T lymphocytes. J Immunol 1981; 127: 1420–1423. [PubMed: 6168690]
14. Meyer CE, Kurth F, Lepore S, et al. In vivo magnetic resonance images reveal neuroanatomical sex differences through the application of voxel-based morphometry in C57BL/6 mice. Neuroimage 2017; 163: 197–205. 2017/09/20. DOI: S1053–8119(17)30775–9 [pii] 10.1016/j.neuroimage.2017.09.027. [PubMed: 28923275]
15. Sawiak SJ, Wood NI, Williams GB, et al. Voxel-based morphometry in the R6/2 transgenic mouse reveals differences between genotypes not seen with manual 2D morphometry. Neurobiology of disease 2009; 33: 20–27. 2008/10/22. DOI: S0969–9961(08)00216–7 [pii] 10.1016/j.nbd.2008.09.016. [PubMed: 18930824]
16. Ashburner J and Friston KJ. Unified segmentation. Neuroimage 2005; 26: 839–851. 2005/06/16. DOI: S1053–8119(05)00110–2 [pii] 10.1016/j.neuroimage.2005.02.018. [PubMed: 15955494]
17. Ashburner J A fast diffeomorphic image registration algorithm. Neuroimage 2007; 38: 95–113. 2007/09/01. DOI: S1053–8119(07)00584–8 [pii] 10.1016/j.neuroimage.2007.07.007. [PubMed: 17761438]

Author Manuscript Author Manuscript Author Manuscript Author Manuscript

18. Hochberg Y and Benjamini Y. More powerful procedures for multiple significance testing. Stat Med 1990; 9: 811–818. 1990/07/01. [PubMed: 2218183]
19. Shattuck DW and Leahy RM. BrainSuite: an automated cortical surface identification tool. Med Image Anal 2002; 6: 129–142. [PubMed: 12045000]
20. MacKenzie-Graham A, Rinek GA, Avedisian A, et al. Cortical atrophy in experimental autoimmune encephalomyelitis: in vivo imaging. Neuroimage 2012; 60: 95–104. 2011/12/21. DOI: S1053–8119(11)01409–1 [pii] 10.1016/j.neuroimage.2011.11.099. [PubMed: 22182769]
21. MacKenzie-Graham A, Tiwari-Woodruff SK, Sharma G, et al. Purkinje cell loss in experimental autoimmune encephalomyelitis. Neuroimage 2009; 48: 637–651. 2009/07/11. DOI: S1053–8119(09)00715–0 [pii] 10.1016/j.neuroimage.2009.06.073.
22. Franklin KBJ and Paxinos G. The Mouse Brain in Stereotaxic Coordinates. 3rd ed. New York: Academic Press, 2008.
23. Porrero C, Rubio-Garrido P, Avendano C, et al. Mapping of fluorescent protein-expressing neurons and axon pathways in adult and developing Thy1-eYFP-H transgenic mice. Brain Res 2010; 1345: 59–72. 2010/06/01. DOI: 10.1016/j.brainres.2010.05.061 S0006-8993(10)01242-4 [pii]. [PubMed: 20510892]
24. Feng G, Mellor RH, Bernstein M, et al. Imaging neuronal subsets in transgenic mice expressing multiple spectral variants of GFP. Neuron 2000; 28: 41–51. 2000/11/22. DOI: S0896–6273(00)00084–2 [pii]. [PubMed: 11086982]
25. Mahad DH, Trapp BD and Lassmann H. Pathological mechanisms in progressive multiple sclerosis. Lancet Neurol 2015; 14: 183–193. 2015/03/17. DOI: 10.1016/S1474-4422(14)70256-X S1474-4422(14)70256-X [pii]. [PubMed: 25772897]
26. Steward O, Zheng B, Ho C, et al. The dorsolateral corticospinal tract in mice: an alternative route for corticospinal input to caudal segments following dorsal column lesions. J Comp Neurol 2004; 472: 463–477. 2004/04/06. DOI: 10.1002/cne.20090. [PubMed: 15065120]
27. Kuang RZ and Kalil K. Specificity of corticospinal axon arbors sprouting into denervated contralateral spinal cord. J Comp Neurol 1990; 302: 461–472. 1990/12/15. DOI: 10.1002/cne.903020304. [PubMed: 1702111]
28. Ghosh A, Peduzzi S, Snyder M, et al. Heterogeneous spine loss in layer 5 cortical neurons after spinal cord injury. Cereb Cortex 2012; 22: 1309–1317. 2011/08/16. DOI: 10.1093/cercor/bhr191 bhr191 [pii]. [PubMed: 21840844]
29. Chen Q, Zheng W, Chen X, et al. Brain Gray Matter Atrophy after Spinal Cord Injury: A Voxel-Based Morphometry Study. Front Hum Neurosci 2017; 11: 211 2017/05/16. DOI: 10.3389/fnhum.2017.00211. [PubMed: 28503142]
30. Kutzelnigg A and Lassmann H. Pathology of multiple sclerosis and related inflammatory demyelinating diseases. Handb Clin Neurol 2014; 122: 15–58. 2014/02/11. DOI: 10.1016/B978-0-444-52001-2.00002-9 B978-0-444-52001-2.00002-9 [pii]. [PubMed: 24507512]
31. Kutzelnigg A, Faber-Rod JC, Bauer J, et al. Widespread demyelination in the cerebellar cortex in multiple sclerosis. Brain pathology (Zurich, Switzerland) 2007; 17: 38–44.
32. Sepulcre J, Sastre-Garriga J, Cercignani M, et al. Regional gray matter atrophy in early primary progressive multiple sclerosis: a voxel-based morphometry study. Arch Neurol 2006; 63: 1175–1180. 2006/08/16. DOI: 10.1001/archneur.63.8.1175. [PubMed: 16908748]
33. Schoonheim MM, Popescu V, Rueda Lopes FC, et al. Subcortical atrophy and cognition: sex effects in multiple sclerosis. Neurology 2012; 79: 1754–1761. 2012/09/29. DOI: 10.1212/WNL.0b013e3182703f46. [PubMed: 23019265]
34. Houtchens MK, Benedict RH, Killiany R, et al. Thalamic atrophy and cognition in multiple sclerosis. Neurology 2007; 69: 1213–1223. 2007/09/19. DOI: 69/12/1213 [pii] 10.1212/01.wnl.0000276992.17011.b5. [PubMed: 17875909]
35. Tambalo S, Peruzzotti-Jametti L, Rigolio R, et al. Functional Magnetic Resonance Imaging of Rats with Experimental Autoimmune Encephalomyelitis Reveals Brain Cortex Remodeling. J Neurosci 2015; 35: 10088–10100. 2015/07/15. DOI: 10.1523/jneurosci.0540-15.2015. [PubMed: 26157006]

Author Manuscript Author Manuscript Author Manuscript Author Manuscript

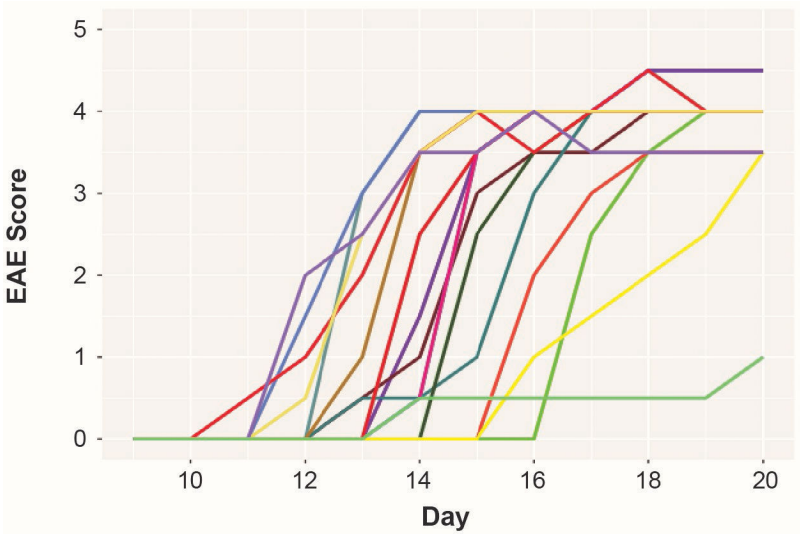

Figure 1.

EAE clinical scores. Mice with EAE (n = 17) demonstrated typical chronic disease using standard EAE scoring while normal control mice (n = 18) displayed no signs of disease. EAE scores for each individual animal are plotted from day 9–20.

Author Manuscript Author Manuscript Author Manuscript Author Manuscript

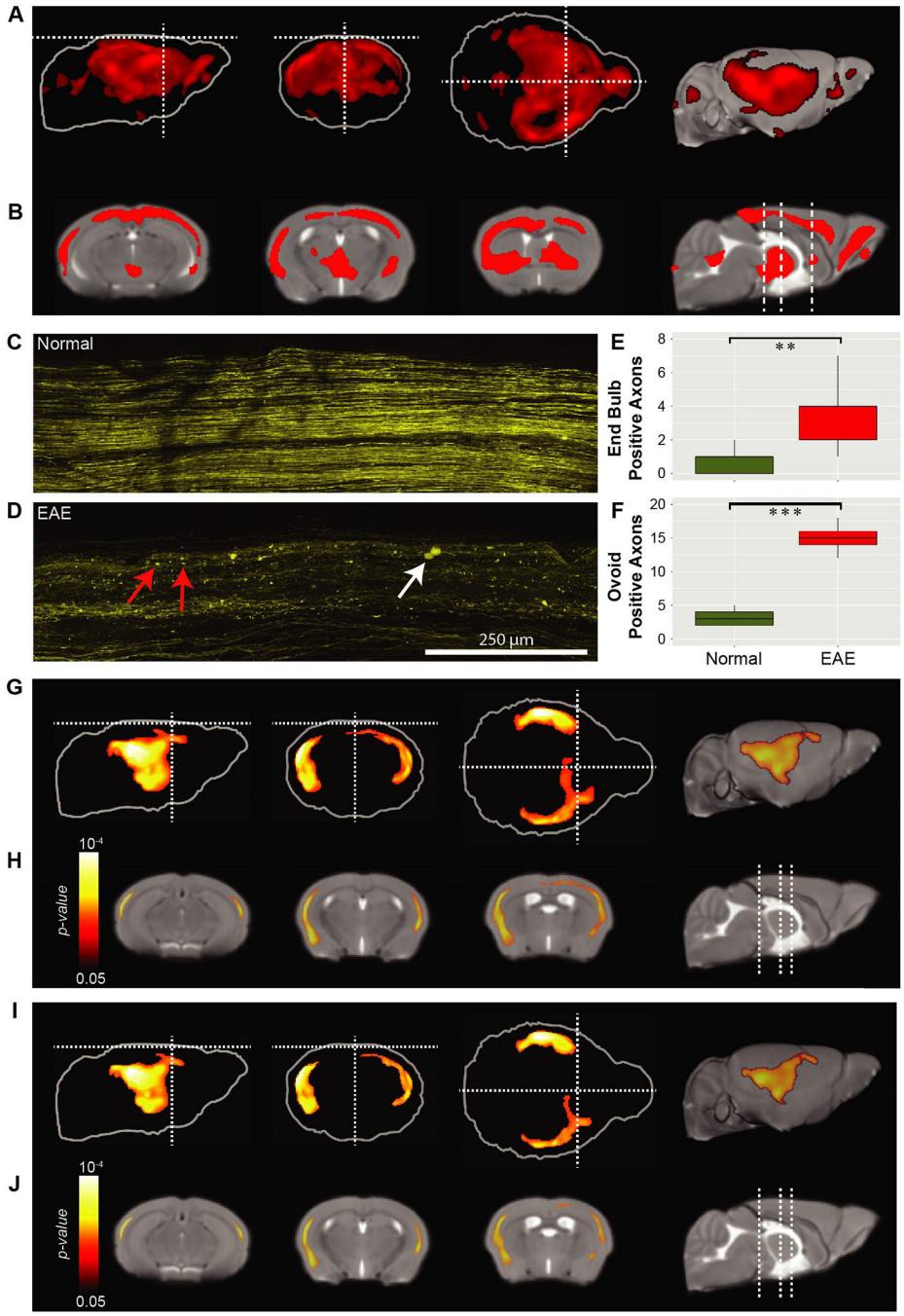

Figure 2.

Axonal transection in the spinal cord correlates with GM atrophy in sensorimotor cortex. A) Maximum intensity projections of GM atrophy in mice with EAE when compared to normal controls ($p < 0.05$, FDR corrected) overlaid on the mean glass brain. The dotted line represents bregma. B) The statistical parametric map indicating GM atrophy in mice with EAE overlaid onto the mean template. The dashed lines represent the location of the representative coronal sections shown from left to right respectively. (n = 18 EAE, 17 normal). C & D) Spinal cords were optically cleared using CLARITY and imaged at 10X

Author Manuscript Author Manuscript Author Manuscript Author Manuscript

magnification. Representative maximum intensity projection images are shown for normal (C) and EAE (D) mice. Scale bar represents 250 μm. E) EAE mice (n = 9) show a significantly larger number of end bulb positive axons than normal mice (n = 9) **($p = 0.0063$). F) EAE mice (n = 9) show a significantly larger number of ovoid positive axons than normal mice (n = 9) ***($p = 1.3 \times 10^{-9}$). G) Maximum intensity projections of the axonal-transection PSA overlaid on the mean glass brain. The colormap indicates regions where axonal transection (end bulbs) in the spinal cord correlated with GM atrophy in the brain ($p < 0.05$, FDR corrected). H) The axonal-transection PSA overlaid on the mean template. (n = 9 EAE, 9 normal). I) Maximum intensity projections of the axonal-injury PSA overlaid on the mean glass brain. The colormap indicates regions where axonal injury (ovoids) in the spinal cord correlated with GM atrophy in the brain ($p < 0.05$, FDR corrected). J) The axonal-injury PSA overlaid on the mean template. (n = 9 EAE, 9 normal).

Author Manuscript Author Manuscript Author Manuscript Author Manuscript

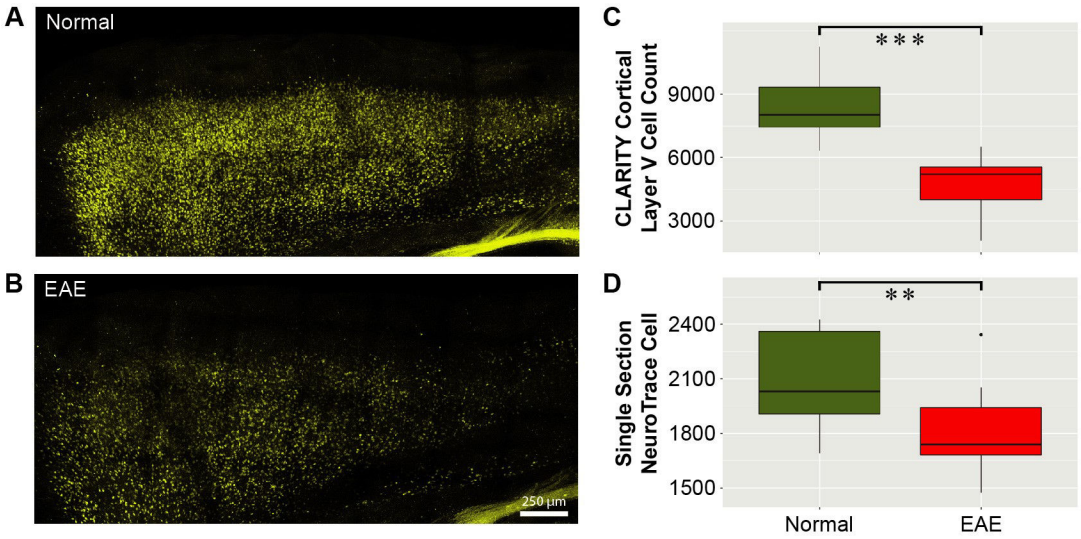

Figure 3.

Reduced cortical layer V neuronal number in sensorimotor cortex during EAE. Brains were optically cleared using CLARITY and imaged at 10X magnification. Representative maximum intensity projection images are shown for normal (A) and EAE (B) mice. Scale bar represents 250 μm. C) Analysis of YFP CLARITY images demonstrated that normal mice (n = 9) have significantly more cortical layer V pyramidal neurons than EAE mice (n = 9) ***(p = 0.00028). D) Normal mice (n = 5) also had significantly more NeuroTrace-positive neurons in serial tissue sections than EAE mice (n = 5) **(p = 0.0063).

Author Manuscript Author Manuscript Author Manuscript Author Manuscript

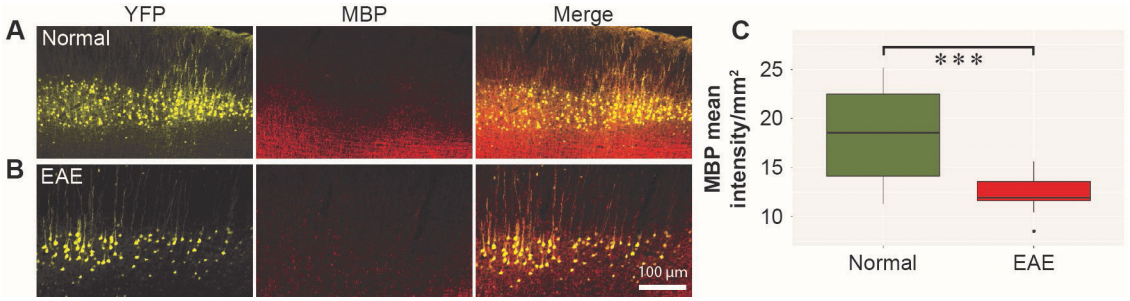

Figure 4.

Demyelination in sensorimotor cortex during EAE. Cortical layer V pyramidal neurons and myelin in the sensorimotor cortex were imaged at 10X in normal (A) and EAE (B) mice. Scale bar represents 100 μm. C) Normal mice (n = 5) demonstrate significantly greater mean MBP staining intensity than mice with EAE (n = 5) ($p = 0.00030$).

Author Manuscript Author Manuscript Author Manuscript Author Manuscript

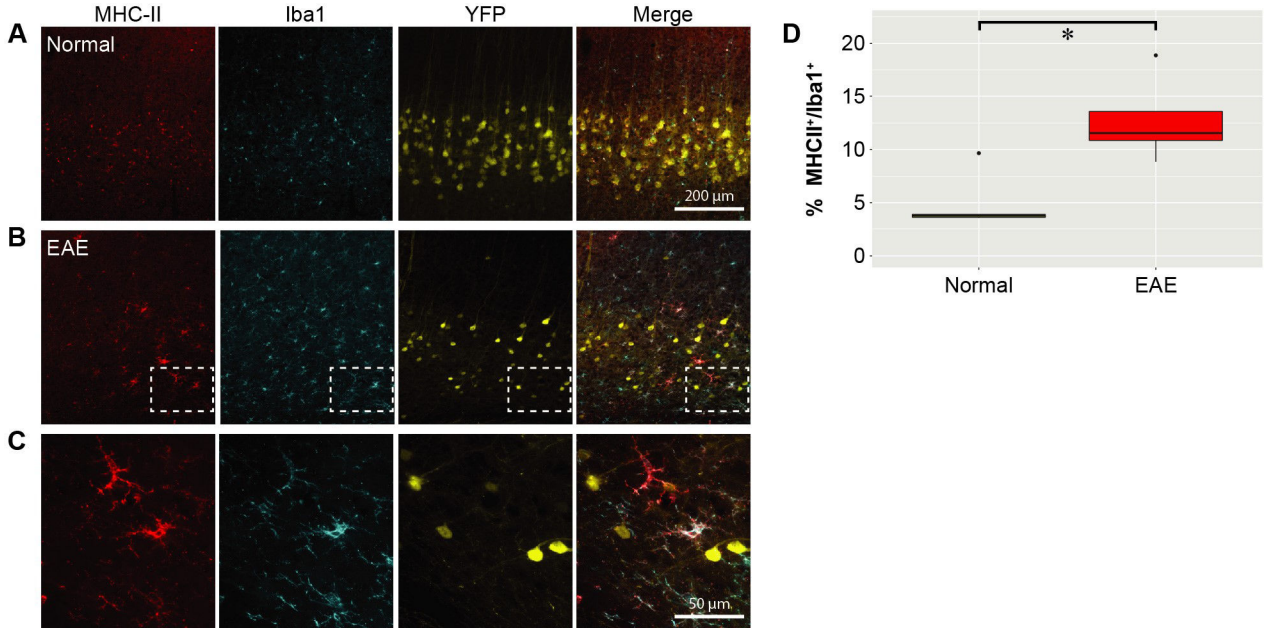

Figure 5.

Activated microglia in sensorimotor cortex in EAE. Iba1 (red), MHC-II (cyan), and cortical layer V pyramidal neurons (yellow) in the sensorimotor cortex were imaged at 10X in normal (A) and EAE (B) mice. Scale bar represents 200 μm. C) 40X image of the area outlined in the EAE images. Scale bar represents 50 μm. D) Normal mice (n = 5) demonstrate significantly less activated microglia than mice with EAE (n = 5) (p = 0.017).

Author Manuscript

Author Manuscript

Author Manuscript

Author Manuscript

Table 1.

Volume comparisons for mice with EAE as compared to normal controls. All reported p-values are FDR-corrected for multiple comparisons. (n = 18 normal, 17 EAE). n.s. indicates not significant.

Region	Mean Volume (mm^3)		Effect Size (mm^3)	*P* value
	Normal	EAE		
Whole brain	435.05 [430.06, 439.89]	425.79 [415.88, 433.74]	n.s.	n.s.
Gray matter	252.96 [248.73, 257.24]	237.77 [231.64, 243.81]	15.20 [7.63, 22.57]	0.00205
White matter	139.87 [137.03, 142.81]	142.67 [139.24, 145.77]	n.s.	n.s.
Cerebrospinal fluid	42.22 [39.79, 44.66]	45.35 [41.91, 48.98]	n.s.	n.s.
Caudoputamen	15.85 [15.68, 16.03]	15.35 [15.14, 15.56]	0.50 [0.22, 0.78]	0.00523
Cerebellum	53.70 [52.99, 54.54]	52.49 [52.02, 52.95]	1.22 [0.34, 2.15]	0.0284
Cerebral cortex	45.39 [44.19, 46.65]	42.01 [40.97, 43.00]	3.38 [1.84, 5.00]	0.00161
Corpus callosum	2.56 [2.47, 2.64]	2.52 [2.48, 2.57]	n.s.	n.s.
Thalamus	13.38 [13.24, 13.52]	13.08 [12.88, 13.26]	0.31 [0.07, 0.55]	0.0342